

# Electromagnetic calorimeter simulation for future $\mu \rightarrow e$ conversion experiments

**Zafar U. Usubov\***

Joint Institute for Nuclear Research,  
Dubna, Russia

December 19, 2012

## Abstract

We examine three dense high-Z scintillating crystals for the  $\mu \rightarrow e$  conversion experiment using the GEANT4 simulation toolkit. The full energy deposition, albedo, and longitudinal and lateral energy leakages for all crystal assemblies are studied. The influence of the crystal depth on the energy deposition in the calorimeter is studied.

## 1 Introduction

Flavor changing by all neutral current interactions is strongly suppressed in the Standard Model(SM) and has not yet been observed. The present values of the neutrino oscillations parameters lead to  $\text{Br}(\mu \rightarrow e\gamma) \leq 10^{-54}$  in the SM. Review of the modern theoretical motivations for lepton flavor violation, data from current experimental bounds and expected improvements astonishingly collected by Marciano, Mori and Roney[1]. Many scenarios beyond the SM (supersymmetry, extra dimensions, little Higgs, quark compositeness) naturally allow and predict some experimentally observable level for processes with charged lepton flavor violation(CLFV). The  $\mu \rightarrow e$  conversion experiments are 10 to 100 times more sensitive to new physics than CLFV searches in other channels. To date the upper limit on the  $\mu^- \rightarrow e^- \gamma$  branching ratio is  $2.4 \cdot 10^{-12}$  at 90% CL[2].

The aim of the  $\mu \rightarrow e$  conversion experiments is to search for the coherent conversion of muons to electrons in the field of a nucleus. Many of the ideas of such experiments are based on a concept that was first proposed by Djilkibaev and Lobashev for the MELC experiment[3], then was developed in MECO[4] project and now formulated in the Mu2e proposal[5].

---

\*On leave of absence from Institute of Physics, Baku, Azerbaijan

At the first step high intense proton beam is directed to the production target. Then pions focused with the graded field produce high-intensity low-energy ( $p_\mu^- < 100 \text{ MeV}$ ) muon beam which serves to create muonic atoms in thin targets. A muon in the orbit could then ordinarily decay or weak capture on the nucleus. For muonic aluminum these processes occur with a probability  $\sim 0.4$  and  $\sim 0.6$ , respectively.

Muon in the orbit can be converted to an electron through some new CLFV interaction with the nucleus. The conversion-to-capture ratio

$$R_{\mu e} = \frac{\Gamma(\mu^- N \rightarrow e^- N)}{\Gamma(\mu^- N \rightarrow \nu_\mu N')}$$

is  $< 6.1(7) \cdot 10^{-13}$  at 90% CL for titanium(gold) nuclei, as obtained in the

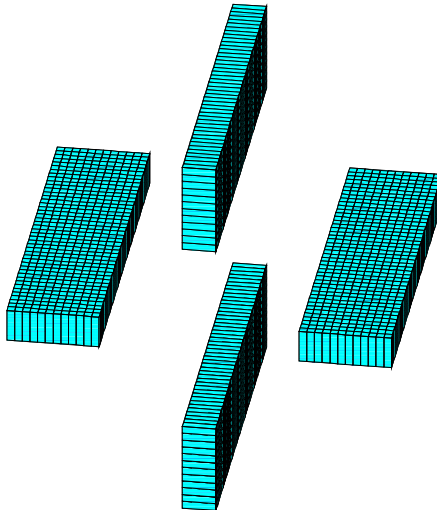


Figure 1: Trigger electromagnetic calorimeter for the Mu2e experiment.

SINDRUM II[6] experiment. For a nominal two-year run ( $2 \cdot 10^7 \text{ s}$ ) the Mu2e experiment could discover about 40 signal events on a background of less than 0.5 events[7]. The expected limit on  $R_{\mu e}$  is  $6 \cdot 10^{-17}$  at 90% CL. This corresponds to the effective mass about  $10^4 \text{ TeV}$ .

In this paper, we explore three dense crystals for the Mu2e trigger calorimeter using the GEANT4[8] simulation toolkit. The next section gives a brief description of the Mu2e experiment setup and the choice of dense crystals for the calorimeter. Section 3 gives our GEANT4 simulation strategy. In this section we present the full energy deposition in the calorimeter, albedo, longitudinal and lateral energy leakages, and the influence of tyvek wrapping on the crystal. We end with the conclusions in Section 4.

Crystal	NaI(Tl)	BGO	LYSO(Ce)	PWO
Density (g/cm <sup>3</sup> )	3.67	7.13	7.40	8.30
Melting Point (°C)	651	1050	2050	1123
Radiation Length (cm)	2.59	1.12	1.14	0.89
Molière Radius (cm)	4.13	2.23	2.07	2.00
Interaction Length (cm)	42.9	22.8	20.9	20.7
Refractive Index	1.85	2.15	1.82	2.20
Hygroscopicity	Yes	No	No	No
Luminescence (nm)(at peak)	410	480	402	425(420)
Decay Time (ns)	245	300	40	30(10)
Light Yield(%)	100	21	85	0.3(0.077)
d(LY)/dT(%/°C)	-0.2	-0.9	-0.2	-2.5

Table 1: Useful characteristics[9] of dense crystals as a Mu2e calorimeter material. The values correspond to the slow or fast(in parentheses) scintillation component.

## 2 Experiment setup and crystal choice

The first stage of the Mu2e experiment will be performed at Fermilab using re-bunched and slow-extracted 8 GeV proton beam from the booster. The Mu2e setup consists of a production solenoid with a production target, a transport

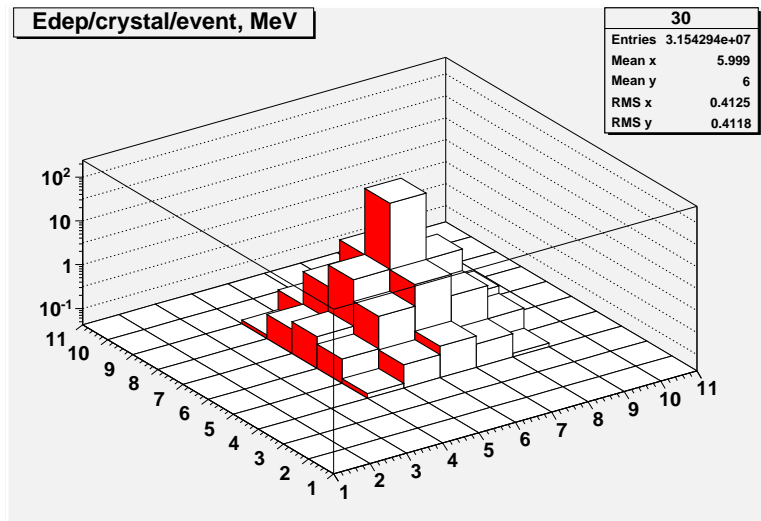


Figure 2: Lego plot for energy deposition in LYSO(Ce) crystals. The electrons with  $E=105$  MeV penetrate the calorimeter perpendicularly.

solenoid with collimators, and a detector solenoid with a stopping target, tracker, and electromagnetic calorimeter. The detector solenoid will provide a highly

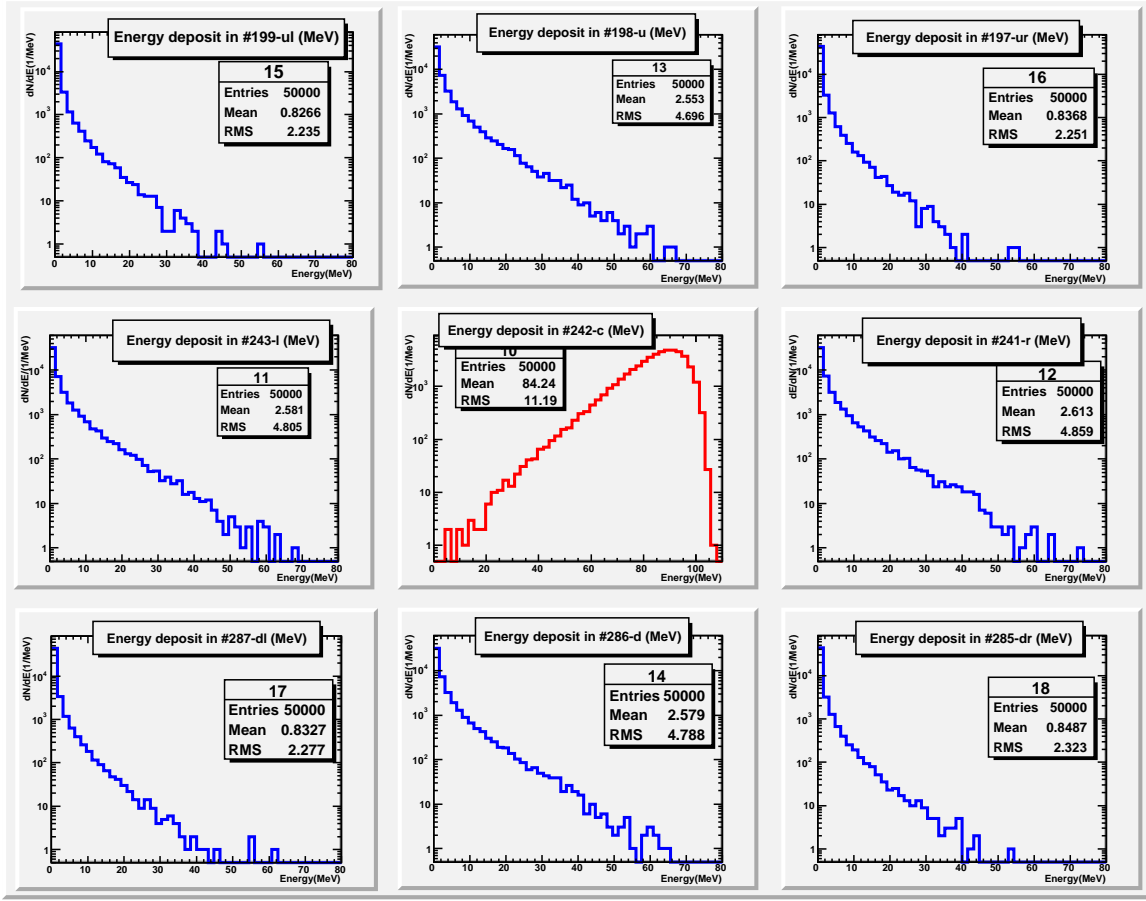


Figure 3: Energy deposition in the central  $3 \times 3$  matrix of the LYSO(Ce) crystals. The electrons with  $E=105$  MeV penetrate the calorimeter perpendicularly.

uniform magnetic field of 1.0 T in tracker and calorimeter area.

The detector of interest is the electromagnetic calorimeter designed as a trigger system, which is also used for measuring (in addition to tracking system) the energy and direction of the conversion electron emitted at the energy  $\sim 105.1$  MeV (for aluminum stopping target). Dense crystals with a short radiation length, small Molière radius, and short decay time can offer good space and time resolution for the calorimeter and allow reduction of the background in the energy window corresponding to the conversion electron.

Crystal scintillators have long been used in nuclear and high-energy physics[10]. Rutherford<sup>1</sup> used ZnS in his alpha-particle scattering study[11], in 1948 Hofstadter<sup>2</sup> first demonstrated NaI(Tl) as a general-purpose detector for photon spectroscopy[12], CsI(Tl) crystals are now used by BELLE, BABAR, BES III,

<sup>1</sup>The Nobel Prize in Chemistry 1908.

<sup>2</sup>The Nobel Prize in Physics 1961, was divided with R.L. Mössbauer.

Crystal	$E_{dep}^8/E_{dep}^9$	$E_{dep}^9/E_{dep}^{all}$
BGO	0.144	0.968
PWO	0.133	0.974
LYSO(Ce)	0.140	0.969

Table 2: The relative energy deposition in the central  $3 \times 3$  matrix of the crystals (see the text).

Crystal	$E_{dep}(MeV)$		Albedo (MeV)		Longitudinal(MeV)		Lateral(MeV)	
	Naked	Wrapped	Naked	Wrapped	Naked	Wrapped	Naked	Wrapped
BGO	101.1	101.2	1.139	1.139	3.184	3.169	1.917	1.735
	5.932	6.031	1.606	1.662	4.403	4.361	1.323	1.406
	50000	50000	39611	39404	46353	47155	370	385
PWO	102.5	102.6	1.150	1.142	2.843	2.824	1.976	2.077
	4.104	4.138	1.512	1.518	3.513	3.410	1.457	1.532
	50000	50000	45896	45837	24042	24798	175	188
LYSO(Ce)	101.0	101.1	0.990	0.982	3.131	3.171	1.981	2.079
	6.080	6.286	1.397	1.449	4.543	4.642	1.770	1.731
	50000	50000	40554	40706	50003	50396	341	413

Table 3: The energy deposition, albedo, and lonitudinal and lateral energy leakages for dense crystals with and without tyvek wrapping (see the text).

and  $PbWO_4$  by CMS and ALICE at the LHC.

Potentially desirable crystals to fully contain electromagnetic showers at the Mu2e experiment energy are lead tungstate  $PbWO_4$ (PWO), bismuth germanate  $Bi_4Ge_3O_{12}$ (BGO), cerium-doped lutetium oxyorthosilicate  $Lu_2SiO_5:Ce$ (LSO(Ce)), and cerium-doped lutetium yttrium oxyorthosilicate  $Lu_{2(1-x)}Y_{2x}SiO_5:Ce$ (LYSO(Ce)). The properties of these crystals are compared with NaI(Tl) in Table 1[9]. This simulation is based on the LYSO crystals which were activated with 0.4% mol of cerium and  $x = 0.1$ .

In the past years oxyorthosilicates was mainly used for medical imaging, namely in the positron emission tomography and mammography scanners (small-size good-quality crystals)[13].

The proposed calorimeter[5] consists of four vanes of detectors(Fig. 1). Each vane considered here comprises  $13 \times 3 \times 3$  cm<sup>3</sup> crystals with the total size  $13 \times 36 \times 132$  cm<sup>3</sup>. Thus, each calorimeter vane consists of 528 cells. The interior faces of the vanes are 39.0 cm away from the solenoid axis. The depth of the calorimeter (13 cm) corresponds to 11.6, 11.4, and 14.6 radiation lengths for the BGO, LYSO(Ce), and PWO crystals, respectively. The electrons are incident on the  $36 \times 132$  cm<sup>2</sup> side of the calorimeter at a mean angle of  $55^\circ$ .

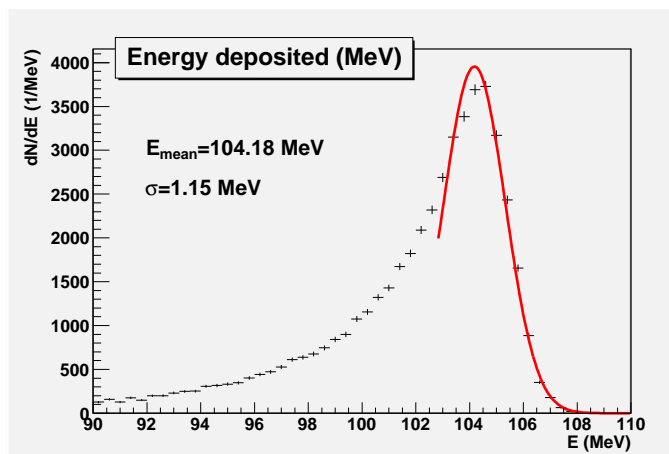


Figure 4: Energy deposition in the calorimeter with the LYCO(Ce) crystals. The electrons with  $E=105$  MeV penetrate the calorimeter perpendicularly.

### 3 Calorimeter simulation and results

The crystal calorimeter simulation is performed with the GEANT4 toolkit using the low-energy physics list. The minimal tracking step was set to  $10\mu\text{m}$ , which corresponds to the energy cuts of  $\sim 3.2$  keV for photons and  $\sim 51.9(50.8)$  keV for electrons(positrons) for the LYSO(Ce) crystals.

We have studied three parts of shower leakage[14]: longitudinal, lateral, and albedo - the backward leakage through the front face of the detector. For each cell, to the energy deposition we added a random energy according to the Gaussian distribution with  $\sigma=1.0$  MeV[15] and  $E_{mean}=0.0$  MeV. The same procedure was applied to the albedo and the tracks leaving the calorimeter in the longitudinal and lateral directions.

In this analysis the optical processes (such as scintillation, refraction, transparency, propagation of light through the crystals towards the light sensors, conversion of the photons into electronic signals) was not considered.

Each analysis was based on 50000 generated events.

The lego plot in Fig. 2 presents the energy deposition in the LYSO(Ce) crystals of the calorimeter vane. The electron beam with  $E=105$  MeV perpendicularly hits at the center of the crystal in the middle of the vane. It is seen that the signal is transversely contained in a  $5\times 5$  matrix. A similar situation is observed for the BGO and PWO crystals.

In Fig. 3 we show the energy deposition in all crystals of the central  $3\times 3$  matrix. Table 2 presents the ratios of energy deposition in eight surrounding

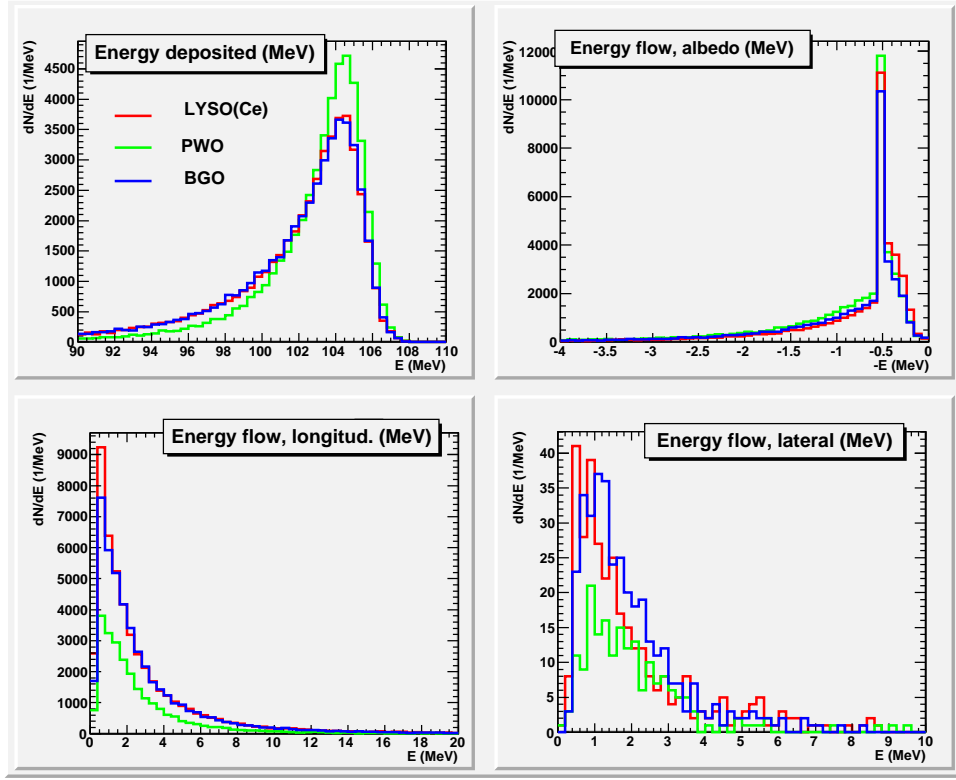


Figure 5: Energy deposition, albedo, and longitudinal and lateral energy leakages for all crystal assemblies. The electrons with  $E=105$  MeV penetrate the calorimeter in the perpendicular direction.

crystals to the energy deposition in all nine crystals in the central  $3 \times 3$  matrix for the BGO, PWO, and LYSO(Ce) crystals. The ratio of the energy deposition in the central  $3 \times 3$  matrix to the total energy deposition in a vane is also presented in the table. We note that most of the 105 MeV electron energy ( $>95\%$ ) is deposited in the central  $3 \times 3$  matrix. The shortest Molière radius of PWO is reflected in the data.

In Fig. 4 the total energy deposition in the calorimeter composed of LYSO(Ce) crystals and irradiated by perpendicularly directed 105 MeV electrons is depicted. The curve corresponding to the Gaussian fit is also shown in the figure. The parameters of the fit are  $E_{mean} = 104.18 \pm 0.012$  MeV and  $\sigma = 1.15 \pm 0.01$  MeV.

Figure 5 compares the total energy deposition, albedo, and longitudinal and lateral energy leakages for the LYSO(Ce), PWO and BGO crystals. The electron beam with the energy of 105 MeV is perpendicularly directed into the central crystal.

In the calorimeters the crystals are usually wrapped in a reflective material to protect them from the light of other crystals. In Table 3 we show the influence of wrapping of the crystals. We modeled the crystals whose lateral faces

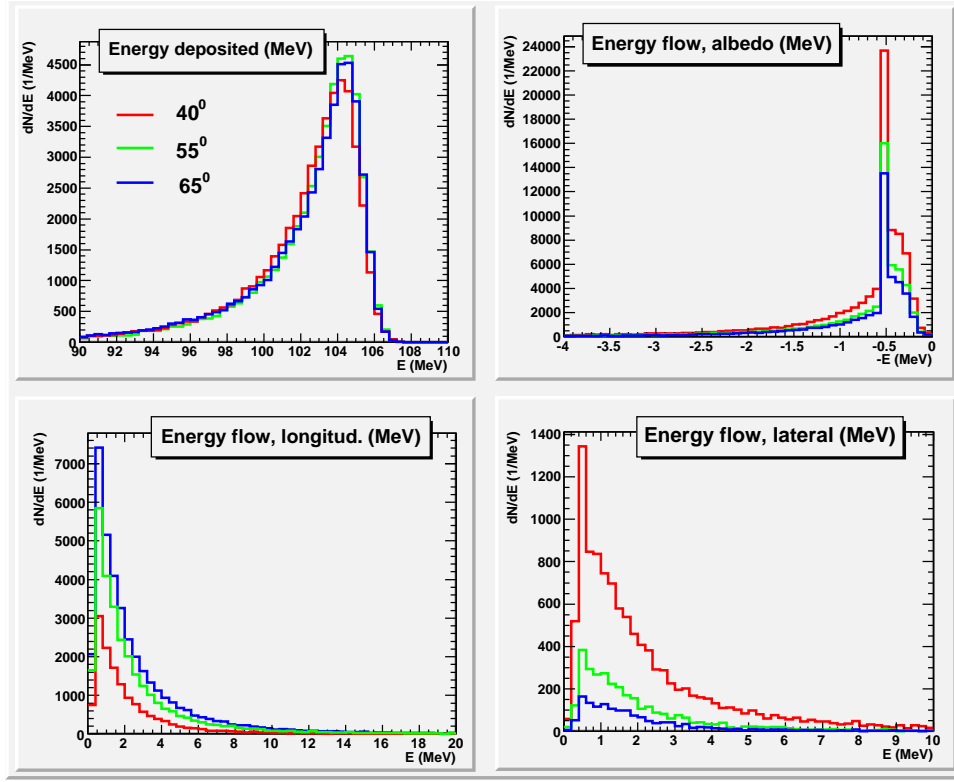


Figure 6: The dependences of the total energy deposition, albedo, and longitudinal and lateral energy leakages on the electron impact angles for the LYSO(Ce) crystals.

were wrapped in 0.1 mm (which corresponds to  $\sim 4$  mil) of tyvek[16] consisting of carbon and hydrogen. The electron beam hits the calorimeter perpendicularly,  $E=105$  MeV. The left(right) column in each table cell corresponds to the naked(wrapped) crystal of the calorimeter. The data in the rows show the mean value(top), root-mean-square(rms) value(middle) and number of entries(lower) for the energy deposition, albedo, and longitudinal and lateral leakages. The data do not show sizable influence of the wrapping since the GEANT4 simulation does not include optical processes.

Note that the lateral energy leakages are almost identical for the crystals, although the number of tracks leaving the PWO crystals is  $\sim 2$  times smaller than in case of BGO and LYSO(Ce).

The electrons in the magnetic field of the tracking solenoid will move in helical trajectories and impact of the calorimeter  $36 \times 132$  cm<sup>2</sup> side with incident angles ranging from  $40^\circ$  to  $65^\circ$ , the mean angle being  $55^\circ$ . In Fig. 6 we display the energy deposition, albedo, and longitudinal and lateral leakages for these three electron impact angles relative to the  $z$  axis (the side of the calorimeter in the  $z$ -direction is 36 cm) for the LYSO(Ce) crystals. Table 4 represents the mean values, rms



Crystal	$E_{dep}(\text{MeV})$			Albedo (MeV)			Longitudinal(MeV)			Lateral(MeV)		
	$40^\circ$	$55^\circ$	$65^\circ$	$40^\circ$	$55^\circ$	$65^\circ$	$40^\circ$	$55^\circ$	$65^\circ$	$40^\circ$	$55^\circ$	$65^\circ$
LYSO(Ce)	101.7	102.0	101.7	1.094	1.040	0.996	2.370	2.761	2.938	2.461	2.134	1.997
	4.931	4.761	5.076	1.878	1.661	1.490	2.945	3.843	4.071	2.614	2.258	1.877
	50000	50000	50000	92618	60112	49816	14221	29338	38488	10965	3210	1453

Table 4: The energy deposition, albedo, and lonitudinal and lateral energy leakages for the calorimeter with the LYSO(Ce) crystals at three different impact angles of 105 MeV electrons.

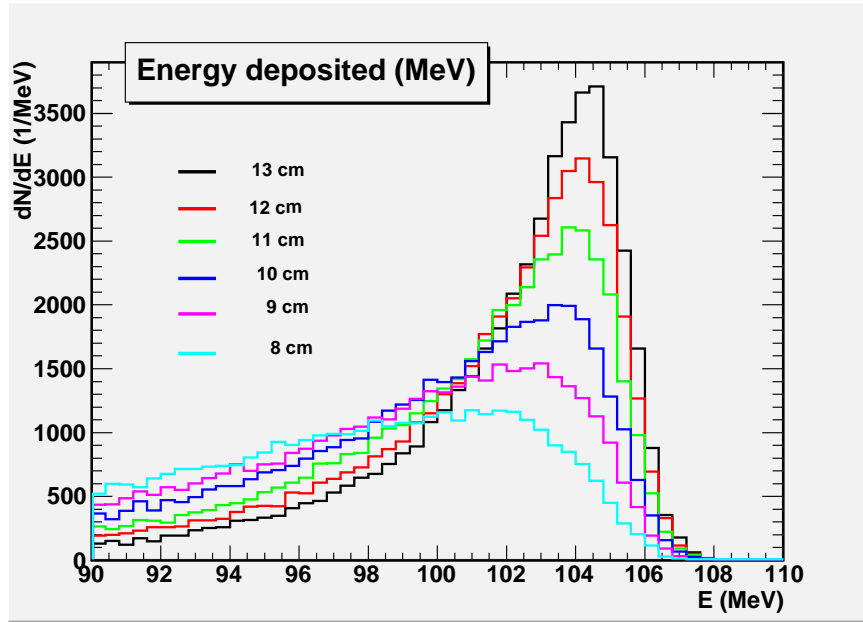


Figure 7: Energy deposition for different LYSO(Ce) crystal depth. The electrons with  $E=105$  MeV penetrate the calorimeter in the perpendicular direction.

values and number of entries for these variables in the first, second and third rows, respectively. Full energy leakages for these impact angles for 105 MeV electrons do not exceed 6% for LYSO(Ce).

Further, we explore the influence of the crystal depth on the energy deposition and energy leakage in the calorimeter. In Fig. 7 we demonstrate the energy deposition for 105 MeV electrons and in Fig. 8 the albedo, longitudinal, and lateral and total energy leakages for the calorimeter with LYSO(Ce) crystals of different depth.

## 4 Conclusions

The ultimate sensitivity and broad new physics motivations make  $\mu \rightarrow e$  coherent conversion a unique channel for charged lepton flavor violating process.

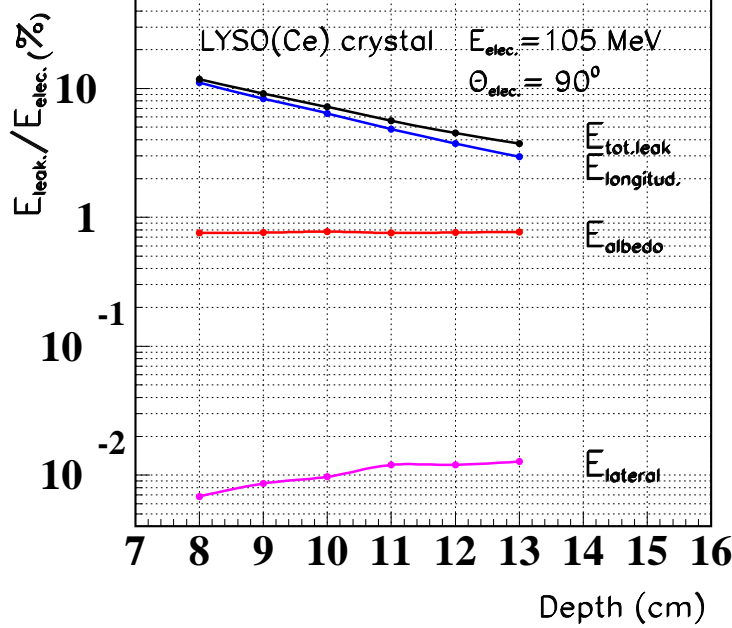


Figure 8: The albedo, longitudinal, lateral, and total energy leakages for the calorimeter with LYSO(Ce) crystals of different depth.

The experiment Mu2e at Fermilab capable of discovering the process or imposing the upper limit as small as  $\sim 2 \cdot 10^{-17}$ , would probe new physics at a mass scale up to  $\sim 10^4 \text{ TeV}$ , much higher than at the LHC.

In this paper we performed short comparison study of dense high-Z PWO, BGO, and LYSO(Ce) crystals as candidates for the Mu2e trigger electromagnetic calorimeter. The study was based on the GEANT4 simulation toolkit. At this stage, all crystals showed attractive behavior to identify the electron in  $\mu \rightarrow e$  conversion.

To accurately simulate the experiment, the processes of scintillation, refraction, transparency, propagation of light through the crystals towards the light sensors and the conversion of photons into electronic signals, etc. must be incorporated in the model. The calorimeter parameters need to be optimized in the full Mu2e experiment setup simulation. The LSO/LYSO crystal bench tests are needed for various readout devices.

We can expect that the high cost of LSO/LYSO crystals ( $\sim 15$ -20 times higher

than PWO crystals) may be significantly reduced if they are mass produced for high-energy physics needs.

## References

- [1] W.J. Marciano, T. Mori, and J.M. Roney, *Annu.Rev.Nucl.Part.Sci.* 58, 315 (2008).
- [2] J. Adam et al., *Phys.Rev.Lett.* 107, 171801 (2011), arXiv:1107.5547 [hep-ex].
- [3] R.M. Djilkibaev and V.M. Lobashev, *Sov.J.Nucl.Phys.* 49(2), 384 (1989); V.S. Abadjev et al., "MELC Experiment to Search for the  $\mu^- A \rightarrow e^- A$  Process", INR Preprint 786/92 (1992).
- [4] M. Bachman et al., "A Search for  $\mu^- N \rightarrow e^- N$  with Sensitivity Below  $10^{-16}$ ", Proposal to BNL, P940, (1997).
- [5] R.M. Carey et al., "Proposal to Search for  $\mu^- N \rightarrow e^- N$  with a Single Event Sensitivity Below  $10^{-16}$ ", FERMILAB-PROPOSAL-0973.
- [6] W. Bertl et al., *Eur.Phys.J.* C47, 337 (2006); C. Dohmen et al., *Phys.Lett.* B317, 631 (1993).
- [7] R.K. Kutschke, *AIP Conf.Proc.* 1182, 718, (2009);  
R.K. Kutschke, "The Mu2e Experiment at Fermilab", arXiv:1112.0242 [hep-ex].
- [8] S. Agostinelli et al., *Nucl.Instr. and Meth.* A506, 250 (2003).
- [9] R. Mao, L. Zhang, R.-Y. Zhu, *IEEE Transactions on Nuclear Science*, v.55, no.4, 2425 (2008).
- [10] M.J. Weber, *Journal of Luminescence* 100, 35 (2002).
- [11] E. Rutherford, J. Chadwich, C.D. Ellis, *Radiation from Radioactive Substances*, Cambridge University Press, Cambridge, 1930.
- [12] R. Hofstadter, *Phys. Rev.* 75, 796 (1949).
- [13] C.W.E. van Eijk, *Radiation Protection Dosimetry*, v.129, no.1-3, 13 (2008).
- [14] R. Wigmans, *Scientifica Acta* 2, No.2, 18 (2008).

- [15] A. Lucà, M. Martini, I. Sara, "GEANT4 Simulation of the Response of a LSO Crystal Electromagnetic Calorimeter to 105 MeV/c Electrons", Mu2e-doc-1080-v3, (2010).
- [16] R. Wojcik et al., Nucl.Instr. and Meth. A342, 416 (1994).